Optimal Placement of Reconfigurable Intelligent Surfaces for Spectrum Coexistence With Radars

Mai Kafafy, Ahmed S. Ibrahim, *Member, IEEE* and Mahmoud H. Ismail, *Senior Member, IEEE*

***Abstract*—In concurrent spectrum sharing scenarios between radars and wireless communication systems, one strict approach to protect the radar from undesired interference is locating the base stations outside a guard (or exclusion) zone of the radar. As a result, users inside that zone experience bad communication coverage. This paper uses Reconfigurable Intelligent Surfaces (RISs) to improve the base station coverage of users in the radar exclusion zone. The paper shows, through analysis and simulation, that joint optimization of base station and RIS locations improves the probability of coverage in the exclusion zone over the shared spectrum without disturbing the radar operation.**

***Index Terms*—Reconfigurable intelligent surfaces, wireless communication, radars, spectrum sharing.**

I. Introduction

One of the important features of 5G and beyond cellular systems is band agility for they are expected to operate on a wide range of licensed and unlicensed spectrum bands [1], [2]. Some of these suggested bands are already occupied by radars (e.g., the 3.55-3.7 GHz Citizens Broadband Radio Service (CBRS) band). Spectrum sharing between radars and communication systems is a promising solution to the increasing demand on wireless services over the crowded RF spectrum. However, spectrum sharing should be orchestrated to have peaceful radar-communication coexistence in which radars remain protected from excessive interference as they are the primary spectrum occupants.

A. Literature Reivew

The literature on radar-communication coexistence is rich with papers that considered different interference management techniques. Examples include opportunistic spectrum access [3]–[5], interference estimation and removal [6], [7], time-frequency resource allocation [8]–[10], and the optimization of transmission parameters such as transmission waveform [11], transmission power [12]–[14], and beamforming [15], [16]. Specifically, [3] considered a cognitive radar that transmits over the least noisy frequency bands that are not used for communication, [4] considered a joint radar-communication transmitter that transmits its radar signal and communication data over disjoint idle spectrum chunks, and [5] considered a set of base stations that are allowed to share the spectrum of a rotating radar only when not in its beam. In addition, [6] and [7] considered a communication receiver that estimates and removes radar interference when decoding communication data. Moreover, [8] and [9] used orthogonal allocation of time-frequency resources to avoid interference between vehicular radars and transceivers, while [10] used non-orthognal channel allocation under interference constraints. Furthermore, [11]–[16] controlled interference levels by optimizing parameters of radar and/or communication transmission. For example, [11] optimized the radar waveform to maximize its Signal to Interference plus Noise Ratio (SINR) subject to constraints on its generated interference over shared communication bands. Papers [12]–[14] optimized the transmission power of a multi-carrier radar and a base station to alternatively maximize the radar mutual information and the base-station capacity in [12], to maximize the base station capacity under constraint on the radar SINR in [13], and to minimize the radar transmission power subject to constraints on the communication capacity and the radar mutual information in [14]. Paper [15] optimized beamforming at a base station to minimize its interference on a nearby radar subject to constraints on the transmission power of the base station and the SINR of its users, wherease [16] optimized the beamforming at a ship borne radar to minimize its interference on a nearby cellular system.

A more strict approach to protect radars from communication interference is setting a radar guard or exclusion zone where concurrent spectrum sharing is not allowed [17]–[19]. Although exclusion zones protect the radar operation, they reduce the communication coverage for User Equipment (UE) located in these zones. In this paper, we propose using Reconfigurable Intelligent Surface (RIS) to enhance coverage inside the radar exclusion zone. RISs are surfaces of electromagnetic materials consisting of a large number of low-cost reflecting elements with configurable phases. Tuning the phases of the RIS reflecting elements passively beamforms the incident signal, and consequently, improves coverage [20]–[22]. Unlike relays, RISs are nearly passive and they can be mounted on walls, windows, billboards, etc.

RIS-assisted communication has a growing literature that considers different optimization objectives and parameters. Most work focused on the optimization of the phases of the

Mai Kafafy is with the Department of Electronics and Communications Engineering, Faculty of Engineering, Cairo University, Giza 12613, Egypt. Email: mai.b.s.ali@eng.cu.edu.eg

Ahmed S. Ibrahim is with the Electrical and Computer Eng. Dept., Florida International University, Miami, FL 33174, USA. Email: aibrahim@fiu.edu.

Mahmoud H. Ismail is with the Department of Electrical Engineering, American University of Sharjah, PO Box 26666, Sharjah, UAE. Email: mhibrahim@aus.edu.

This work was supported by the American University of Sharjah under Grants no. EN0281:SCRI18-07 and FRG20-M-E10. The work of Ahmed S. Ibrahim was supported in part by the National Science Foundation under Award CNS-2144297.

RIS (i.e., passive beamforming) and transmit beamforming at the base station to maximize different system objectives. For example, [23], [24] maximized the RIS-assisted rate where [23] focused on a single user MISO (Multi Input Single Output) link, while [24] adopted a multi user MISO setup with water-filling like power allocation. References [25], [26] maximized the spectral efficiency of a single RIS-assisted MISO and Multi Input Multi Output (MIMO) link, respectively. In addition, [27] maximized the SINR received at a specific user by optimizing a three dimensional transmit beamform at the base station jointly with the passive beamform at the RIS. Moreover, [28] maximized the energy efficiency of a system of base station and multiple RISs. Furthermore, [29] minimized the symbol error probability in a single RIS-assisted MIMO link. Finally [30] minimized the base station transmit power in a multi-user MISO broadcast setup.

Vehicular systems with RISs installed on the roadside and on buildings to improve vehicle to infrastructure (V2I) communication were addressed in [31]–[34]. Specifically, [31] showed through analysis that RIS-assisted communication reduces the outage probability on a two-lane road model. Reference [32] optimized RIS phases to maximize the uplink V2I rate, [33] optimized RIS phases and vehicle scheduling to maximize the minimum average V2I bit-rate, and [34] optimized resource allocation and RIS phases to maximize the V2I sum rate. In addition, communication systems with RISs and Unmmaned Aerial Vehicles (UAVs) were considered in [35]–[37]. To elaborate, [35] considered a ground RIS that beamforms the signal of a UAV to a ground user, and optimized the RIS phases and the UAV trajectory to maximize the user rate. Reference [36] showed the reduction in outage probability when a ground RIS phase modulates the signal of an RF transmitter and a UAV relays the modulated signal to a remote ground destination. Moreover, [37] suggested mounting RISs on aerial platforms to extend coverage to remote ground areas, and [38], [39] suggested mounting RISs on low earth orbiting satellites to enhance inter-satellite communication. Recently, stochastic geometry was used in [40], [41] to derive the probability of coverage in a cellular system with random RIS deployment. In [40] electrically large RISs were assumed to redirect the base station signal beyond obstacles, while in [41] diffuse RISs were assumed to beamform the base station signal to the served UE.

The papers discussed above have a common assumption that the location of the RISs are either known or random. The optimization of RIS placement was less considered in literature. For example, [42] optimized the RIS location to minimize the joint probability of blocking the direct and the indirect path between a user and a base station, [43] optimized the RIS location to maximize the received signal between a transmitter and a receiver considering the beam footprint of highly directive link on the RIS, and [44] optimized the RIS orientation and horizontal distance from the base station to maximize the cell coverage. In addition, [45] optimized the one dimensional placement of RISs on road to maximize the signal received by a vehicle from road size units, [46] optimized the phases and location of an aerial RIS to maximize the minimum SNR achieved in an obstructed region, and [47] optimized the phases and trajectory of aerial RIS to maximize the downlink rate of a mobile user.

RIS deployment in radar-communication scenarios was only considered in few papers that optimized the RIS phases not placement [48]–[50]. To specify, [48], [49] considered a base station with dual radar-communication function where [48] optimized the transmit precoding matrix and the phases of the RIS to maximize the radar detection performance under signal to noise ratio and power constraints, while [49] divided the RIS elements for localization and communication. On the other hand, [50] considered coordinated radar-communication coexistence where a base station and a radar are integrated through a central control unit. The paper optimized the transmit beamforming of the base sation and the RIS phases to maximize radar detection probability under constraints on the communication performance; however, the effect of RIS deployment on the radar performance (e.g., self interference) was not considered.

B. Contribution

In this paper, we propose using RIS to improve base station coverage of UEs located in the exclusion zone of a nearby radar. RISs are advantageous as they are nearly passive and able to beamform the incident signals; however, their operation on a shared spectrum with a nearby radar has its challenges for two main reasons. Firstly, while the RIS creates a beamformed channel between the base station and its UEs, it also creates extra scattering channels between the radar and the UEs and between the base station and the radar, which increases interference at both the UEs and the radar. Secondly, the RIS location affects the performance of both the communication and the radar systems as it affects the received signal at both the UE and the radar. Thus, careful placement of the RIS is necessary in order to benefit the communication system without jeopardizing the operation of the nearby radar.

To the best of our knowledge, this paper is the first to consider the deployment of RIS-assisted communication and optimizing RIS-base station placement to improve coverage in the presence of a nearby radar with an exclusion zone. The contributions of the paper are, thus, summarized as follows:

- Analyzing the effect of RIS deployment on the communication performance by deriving the probability of coverage with and without the RIS.
- Analyzing the effect of RIS on the radar performance by deriving the probability of target detection with and without the RIS.
- Optimizing the locations of the base station and the RIS to maximize the communication coverage of UEs in the radar exclusion zone without affecting the radar performance.

Our analysis and simulation results show that optimized RIS-assisted communication improves coverage of UEs in the radar exclusion zone while keeping the radar performance unharmed. We also show that the optimum locations of the RIS and the base stations depend on a number of parameters including the UEs distribution and the frequency of signal obstruction.

The rest of this paper is organized as follows: we first start by presenting the system model in Section II, the effect of RIS on the communication and radar performance is then analyzed in Sections III and IV. The placement optimization of the RIS and the base station is then formulated and solved in Section V. The results are presented in Section VI before the paper is finally concluded in Section VII.

II. System Model

A. Network Model

Consider a network model with a rotating mono-static pulsed radar is located at the origin, and base stations that are only allowed outside the radar exclusion zone. RISs are allowed inside the exclusion zone to enhance the base station coverage of users inside the zone. Base stations and RISs can have irregular placement or regular placement on a grid structure (e.g., hexagonal grid). As discussed in [51], the analysis of RIS-assisted communication is challenging and the system performance metrics do not usually come in closed forms [41]. This is because the received signal and interference levels at a typical UE depend not only on the direct links between the UE and the base stations, but also on the indirect paths through different RISs. The analysis of RIS-assisted communication in the vicinity of a radar is even more challenging as the network is no longer symmetric around the UE due to the exclusion zone and the radar rotation. Consequently, inspired by [42], [52], we adopt the simplified one-dimensional model shown in Fig. 1 as it is important for mathematical tractability. We believe that a tractable analysis provides good insights into the benefits and limitations of RIS-assisted communication in the vicinity of a radar, especially that this is the first work to consider such a system. The simplified model can also be considered a good approximation for vehicle-to-infrastructure (V2I) communication on roads [45]. A stochastic geometry based analysis of a two-dimensional system is left for future work.

Now, consider a one-dimensional network as shown in Fig. 1 with a mono-static rotating pulsed radar located at the origin. The peak transmission power of the radar is denoted by p_r and its search range by d. A base station, with a downlink transmit power p_c, shares the radar spectrum and is located at a guard distance z from the radar, which is decided by the radar to protect it from base station interference. An RIS with K reflecting elements is located at distance $r = a \times z$ from the radar, where $0 < a < 1$ to ensure that the RIS is located between the radar and the base station. A typical UE, randomly located at $0 \leq U \leq z$, receives the direct base station signal and a beamformed signal from the RIS as shown in Fig. 1. The RIS passively beamforms the impinging base station signal to the served UE by tuning the phases of its K reflecting elements.

B. Channel Models

This subsection represents the statistical characterization of the direct and indirect channels, through the RIS, between different entities in the network.

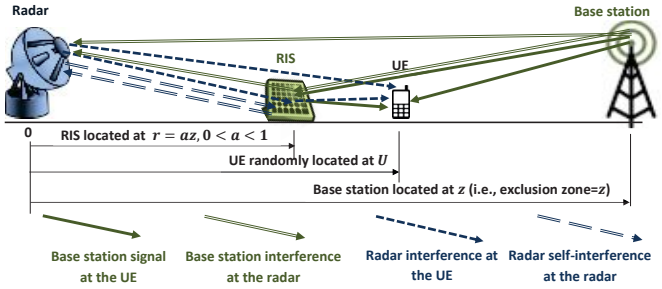

Fig. 1. A one-dimensional model of RIS-assisted communication near a radar.

1) direct channels: We assume that all direct channels experience slow flat Rayleigh fading [41], such that all direct channels follow a Circularly Symmetric Complex Gaussian (CSCG) distribution $\mathcal{CN}(0, 1/2)$. Let h denote the direct channel between the base station and the UE, h^r denote the direct channel between the radar and the UE, and $\tilde{h}$ denote the direct channel between the radar and the base station. Also, let $\hat{h}_k$ ($\hat{h}_k^r$) denote the direct channel between the base station (radar) and the kth reflecting element of the RIS and $\check{h}_k$ denote the direct channel between the kth reflecting element of the RIS and the UE.

2) indirect channels through the RIS: The channel from the base station to the UE through the RIS is denoted by g and is calculated as follows [41]:

$$g = \sum_{k=1}^{K} \hat{h}_k e^{j\phi_k} \check{h}_k = \sum_{k=1}^{K} |\hat{h}_k||\check{h}_k| e^{j\left(\phi_k + \angle \hat{h}_k + \angle \check{h}_k\right)}, \tag{1}$$

where $|\cdot|$ and $\angle\cdot$ denote the magnitude and phase, respectively, and the vector $\boldsymbol{\phi} = \begin{bmatrix} \phi_1 & \phi_2 & \cdots & \phi_K \end{bmatrix}^T$ is the phase vector of the K reflecting elements of the RIS.

Now, the RIS reinforces downlink communication as it beamforms the base station signal to the UE by tuning the phases of its reflecting elements such that the beamformed base station signal is aligned with the direct base station signal at the UE (i.e., $\phi_k + \angle \hat{h}_k + \angle \check{h}_k = \angle h$). We denote the beamformed channel from the base station to the UE through the RIS by g^*, which takes the form [41]

$$g^* = e^{j\angle h} \sum_{k=1}^{K} |\hat{h}_k||\check{h}_k|. \tag{2}$$

Since the RIS usually has a large number of elements and from the Central Limit Theorem (CLT), $|g^*|$ can be approximated by a Gaussian random variable (r.v.) that has the Probability Density Function (PDF)

$$f_{|g^*|}(g) = \frac{1}{\sqrt{2\pi\sigma_{g^*}^2}} \exp\left(-\frac{(g-\mu_{g^*})^2}{2\sigma_{g^*}^2}\right), \tag{3}$$

where $\mu_{g^*} = K\mathbb{E}\left[|\hat{h}_k||\check{h}_k|\right]$ and $\sigma_{g^*}^2 = K\text{Var}\left[|\hat{h}_k||\check{h}_k|\right]$, with $\mathbb{E}[\cdot]$ being the expectation operator and $\text{Var}[\cdot]$ denoting the variance. From the analysis of double rayleigh channels in [41], [53], μ_{g^*} and $\sigma_{g^*}^2$ are given by

$$\mu_{g^*} = K\frac{\pi}{4}, \quad \sigma_{g^*}^2 = \left(1 - \frac{\pi^2}{16}\right) K. \tag{4}$$

Since the phases of the RIS are not tuned to beamform the signal from the radar to the UE, the phases are considered random and the RIS scatters the signal. Consequently, the channel between the radar and the UE, denoted by g^r, can be approximated using the CLT as a CSCG $\mathcal{CN}(0, K/2)$ (see Proposition 2 in [41]). The same approximation can be applied to the channel between the base station and the radar, denoted by $\tilde{g}^r$, and the channel experienced by the radar signal that is scattered from the RIS back to the radar, denoted by g^{rr}, such that $\tilde{g}^r \sim \mathcal{CN}(0, K/2)$ and $g^{rr} \sim \mathcal{CN}(0, K)$.

C. Received Signals

The signal received at the UE, denoted by $R^c(t)$, is given by

$$R^c(t) = \frac{\lambda\sqrt{p_c G_c}}{4\pi}\left(|h| d_0^{-\frac{\alpha}{2}} + |g^*|(\hat{d}\check{d})^{-\frac{\alpha}{2}}\right) e^{j\angle h} T^c(t) + \frac{\lambda\sqrt{\bar{p}_r G_r}}{4\pi}\left(h^r U^{-\frac{\alpha}{2}} + g^r (r\check{d})^{\frac{-\alpha}{2}}\right) T^r(t)\delta^r(t) + n^c(t), \tag{5}$$

where $T^c(t)$ and $T^r(t)$ are the transmit signals of the base station and the radar, respectively, G_c is the base station antenna power gain, λ is the wavelength, α is the pathloss exponent. The first term in (5) represents the base station signal received through the direct path and the RIS where $d_0 = z - U$ is the distance between the base station and the UE, $\hat{d} = z - r$ is the distance between the base station and the RIS, and $\check{d} = |r - U|$ is the distance between the RIS and the UE. The second term, on the other hand, represents the interfering radar signal received through the direct path and through the RIS. Also, $\bar{p}_r = p_r T_p \nu$ is the average observed power of a pulsed radar where T_p is the pulse duration and ν is the pulse repetition frequency. $\delta^r(t)$ is a binary function that takes the value 1 if the UE is in the beam of the rotating radar and 0 otherwise. Finally, the term $n^c(t)$ represents the additive white Gaussian noise (AWGN) with zero mean and variance $\tilde{\sigma}_n^2$.

Similarly, the signal received at the radar receiver, denoted by $R^r(t)$, consists of

$$R^r(t) = \sqrt{\frac{p_r G_r^2 \lambda^2 \Omega}{(4\pi)^3}} d^{-2} T^r(t) + \sqrt{\frac{p_c G_c G_r \lambda^2}{(4\pi)^2}}\left(\tilde{h} z^{-\frac{\alpha}{2}} + \tilde{g}(\hat{d}r)^{-\frac{\alpha}{2}}\right) T^c(t) + \sqrt{\frac{\bar{p}_r G_r^2 \lambda^2}{(4\pi)^3}} g^{rr} r^{-\alpha} T^r(t) + n^r(t), \tag{6}$$

where the first term is the radar signal reflected from an aerial target that has a radar cross section Ω at distance d from the radar, the second term is the base station interference received at the radar through the direct link and the RIS and the third term is the radar signal scattered from the RIS. Finally, the term $n^r(t)$ represents the AWGN with zero mean and variance $\tilde{\sigma}_n^2$. In the above equation, we assume that the signal reflected from the aerial target on the indirect path through the RIS is negligible due to the longer propagation distance, and hence the higher path loss, as RISs are usually installed at lower levels than aerial targets [50].

III. Communication Performance Analysis

In this section, we analyze the RIS effect on the probability of coverage of UEs that are located in the radar protection region. In particular, we derive the probability of coverage in the absence of an RIS in Section III-A and in the presence of an RIS in Section III-B.

A. Probability of Coverage Without an RIS

In this subsection, we consider a traditional communication model (i.e., without an RIS) where the desired base station signal and the unwanted radar interference are received through the direct links between the base station, the radar, and the UE. The SINR at a UE located at a distance U from the radar in the absence of an RIS is denoted by β_U^0 and has the following form:

$$\beta_U^0 = \frac{p_c G_c |h|^2 {d_0}^{-\alpha}}{\sigma_n^2 + I_{r\to u}^0}, \tag{7}$$

where the numerator is from the direct (first) component of the base station signal $T^c(t)$ in (5) and the denominator is the noise term $\sigma_n^2 = (4\pi)^2/\lambda^2\tilde{\sigma}_n^2$ added to $I_{r\to u}^0$, which is the direct radar interference at the UE. $I_{r\to u}^0$ comes from the direct (second) component of the radar signal $T^r(t)$ in (5) as follows

$$I_{r\to u}^0 = \begin{cases} \bar{p}_r G_r |h^r|^2 U^{-\alpha}, & \text{with prob. } \tau, \\ 0, & \text{with prob. } 1-\tau. \end{cases} \tag{8}$$

As seen in (8), the interference at the UE depends on the radar direction relative to the UE position. Specifically, the parameter τ in (8) is the time portion when the UE is in the radar direction, which depends on the radar beamwidth as well as its full scan time. Unlike traditional communication systems, the randomness in $I_{r\to u}^0$ should be considered when calculating the probability of coverage over a shared radar spectrum. The probability of coverage of the UE, denoted by η_u^0, is the probability that the SINR β_u^0 exceeds some threshold $\tilde{\beta}$ (i.e., $\eta_U^0 = P(\beta_U^0 \geq \tilde{\beta})$, which is calculated as follows

$$\begin{aligned} \eta_U^0 &= (1-\tau) P\left(|h|^2 \geq \frac{\tilde{\beta} d_0^\alpha}{p_c G_c}\sigma_n^2\right) + \\ &\tau \mathbb{E}_{|h^r|^2}\left[P\left(|h|^2 \geq \frac{\tilde{\beta} d_0^\alpha}{p_c G_c}\left(\sigma_n^2 + \bar{p}_r G_r |h^r| U^{-\alpha}\right)\right)\right] \\ &\overset{a}{=} \exp\left(\frac{-\tilde{\beta} d_0^\alpha \sigma_n^2}{p_c G_c}\right)\left((1-\tau) + \right. \\ &\left.\tau \mathbb{E}_{|h^r|^2}\left[\exp\left(\frac{-\tilde{\beta} d_0^\alpha \bar{p}_r G_r}{p_c G_c U^\alpha}|h^r|^2\right)\right]\right) \\ &\overset{b}{=} \exp\left(\frac{-\tilde{\beta} d_0^\alpha \sigma_n^2}{p_c G_c}\right)\left((1-\tau) + \frac{\tau}{1 + \frac{\tilde{\beta}\bar{p}_r G_r}{p_c G_c}\left(\frac{d_0}{U}\right)^\alpha}\right). \end{aligned} \tag{9}$$

The first (second) term of (9) averages over the case when the UE is (is not) in the radar direction and the expectation operator is over $|h^r|^2$, which is the power gain of the direct

channel between the radar and the UE. In addition, the line $\stackrel{a}{=}$ results from substituting with the complementary cumulative distribution function (CDF) of $|h|^2$, the power gain of the direct channel between the base station and the UE, which is an exponential r.v. with mean 1 since we assume Rayleigh-faded direct channels in Section II-B. Finally, the line $\stackrel{b}{=}$ is a result of averaging over $|h^r|^2$, which is also an exponential r.v. with mean 1.

B. Probability of Coverage With an RIS

In this subsection, we consider a beamforming RIS located at r as explained in the system model. Unlike the previous subsection, a UE receives the base station signal combined from the direct and the indirect paths through the RIS. Similarly, an additional component of the radar interference is received at the UE because of the scattered radar signal through the RIS. The SINR of the UE in the presence of an RIS is denoted by β_U^1 and takes the following form:

$$\beta_U^1 = \frac{p_c G_c |f|^2}{\sigma_n^2 + I_{r\to u}^1}, \tag{10}$$

where the numerator is the beamformed base station signal from the direct and the indirect paths. In the denominator, the term $I_{r\to u}^1$ is the combined radar interference at the UE given by

$$I_{r\to u}^1 = \begin{cases} \bar{p}_r G_r |f^r|^2, & \text{with prob. } \tau, \\ 0, & \text{with prob. } 1-\tau, \end{cases} \tag{11}$$

where $|f^r|^2$ is the combined direct and indirect scattering channels (i.e., through the RIS) between the radar and the UE. It is obtained from the $T^r(t)$ term in (5) as follows

$$|f^r|^2 = |U^{-\frac{\alpha}{2}} h^r + \left(r\check{d}\right)^{-\frac{\alpha}{2}} g^r|^2. \tag{12}$$

Knowing from Subsection II-B that $h^r \sim \mathcal{CN}(0,1)$ and that $g^r \sim \mathcal{CN}(0,K)$, then $|f^r|^2$ is an exponential r.v. with mean $\left(U^{-\alpha} + K(r\check{d})^{-\alpha}\right)$.

Going back to (10), $|f|^2$ represents the combined direct and indirect beamformed channels between the base station and the UE. It is obtained from the $T^c(t)$ term in (5) as follows

$$\begin{aligned} |f|^2 &= \left(|h| d_0^{-\frac{\alpha}{2}} + |g^*| \left(\hat{d}\check{d}\right)^{-\frac{\alpha}{2}}\right)^2 \\ &= d_0^{-\alpha}|h|^2 + 2\left(d_0 \hat{d}\check{d}\right)^{-\frac{\alpha}{2}} |h||g^*| + |g^*|^2 \left(\hat{d}\check{d}\right)^{-\alpha}. \end{aligned} \tag{13}$$

According to [41], the combined channel between a base station and a UE in RIS-assisted communication can be characterized by the Gamma distribution whose scale and shape parameters w and v are, respectively, given by

$$w = \frac{\mathbb{E}\left[|f|^4\right] - \mathbb{E}^2\left[|f|^2\right]}{\mathbb{E}^2\left[|f|^2\right]}, \tag{14}$$

$$v = \frac{\mathbb{E}\left[|f|^2\right]}{w}, \tag{15}$$

where $\mathbb{E}\left[|f|^2\right]$ is the first moment of $|f|^2$ given as [41]

$$\mathbb{E}\left[|f|^2\right] = \frac{1}{d_0^\alpha} + \frac{\mu_{g^*}^2 + \sigma_{g^*}^2}{(\hat{d}\check{d})^\alpha} + \sqrt{\frac{\pi}{(\hat{d}\check{d})^\alpha}}, \tag{16}$$

and $\mathbb{E}\left[|f|^4\right]$ is its second moment, which has the following form [41]

$$\begin{aligned} \mathbb{E}\left[|f|^4\right] &= \frac{2}{d_0^{2\alpha}} + \frac{3K\pi^{\frac{3}{2}}}{4 d_0^{\frac{3\alpha}{2}} \left(\hat{d}\check{d}\right)^{\frac{\alpha}{2}}} + \frac{6(\mu_{g^*}^2 + \sigma_{g^*}^2)}{d_0^\alpha \left(\hat{d}\check{d}\right)^\alpha} \\ &+ \frac{2\sqrt{\pi}}{d_0^{\frac{\alpha}{2}} \left(\hat{d}\check{d}\right)^{\frac{3\alpha}{2}}} \left(\frac{\pi^3 K^3}{64} + \frac{3}{4}\pi K^3 \left(1 - \frac{\pi^2}{16}\right)\right) \\ &+ \frac{1}{\left(\check{d}\hat{d}\right)^{2\alpha}} \left(\frac{\pi^4 K^4}{256} + \frac{\pi^2 K^3}{4}\left(1 - \frac{\pi^2}{16}\right) + 3K^3\left(1 - \frac{\pi^2}{16}\right)\right). \end{aligned} \tag{17}$$

Following the same approach to deriving the probability of coverage in Subsection III-A, the RIS-assisted probability of coverage of a UE at a distance U from the radar is denoted by η_U^1 and is defined as $\eta_U^1 = P(\beta_U^1 \geq \tilde{\beta})$, which is calculated as follows

$$\begin{aligned} \eta_U^1 &= (1-\tau) P\left(|f|^2 \geq \frac{\tilde{\beta} d_0^\alpha}{p_c G_c} \sigma_n^2\right) + \tau \times \\ &\mathbb{E}_{|f^r|^2}\left[P\left(|f|^2 \geq \frac{\tilde{\beta} d_0^\alpha}{p_c G_c}\left(\sigma_n^2 + \bar{p}_r G_r |f^r| U^{-\alpha}\right)\right)\right] \\ &\stackrel{a}{=} (1-\tau)\left(1 - \frac{1}{\Gamma(v)}\gamma(v, \frac{\tilde{\beta}\sigma_n^2}{p_c G_c w})\right) + \\ &\tau\left(1 - \mathbb{E}_{|f^r|^2}\left[\frac{1}{\Gamma(v)}\gamma(v, \frac{\tilde{\beta}}{p_c G_c w}(\sigma_n^2 + \bar{p}_r G_r |f^r|^2)\right]\right), \end{aligned} \tag{18}$$

where $\stackrel{a}{=}$ follows by substituting with the complementary CDF of the gamma-distributed $|f|^2$, $\Gamma(\cdot)$ is the gamma function and $\gamma(\cdot,\cdot)$ is the lower incomplete gamma function. To put the probability of coverage in (18) in a closed form, we substitute with the power series expansion of the lower incomplete gamma function as follows:

$$\begin{aligned} &\mathbb{E}_{|f^r|^2}\left[\gamma\left(v, \frac{\tilde{\beta}}{p_c G_c w}\left(\sigma_n^2 + \bar{p}_r G_r |f^r|^2\right)\right)\right] \\ &\stackrel{a}{\approx} \mathbb{E}_{|f^r|^2}\left[\gamma\left(v, \frac{\tilde{\beta}\bar{p}_r G_r}{p_c G_c w}|f^r|^2\right)\right] \\ &= \sum_{n=0}^{\infty} \frac{1}{\Gamma(v+n+1)} \mathbb{E}_\zeta[e^{-\zeta}\zeta^{n+v}] \\ &\stackrel{b}{=} \sum_{n=0}^{\infty} \frac{1}{\Gamma(v+n+1)} \frac{(n+v)!}{\lambda_\zeta (1+\frac{1}{\lambda_\zeta})^{n+v+1}} \end{aligned} \tag{19}$$

where $\stackrel{a}{\approx}$ is a result of neglecting the noise power compared to the radar interference and $\stackrel{b}{=}$ results from averaging over ζ where $\zeta = \frac{\tilde{\beta}\bar{p}_r G_r}{p_c G_c w}|f^r|^2$ is an exponential r.v. with mean $\lambda_\zeta = \frac{\tilde{\beta}\bar{p}_r G_r}{p_c G_c w}(U^{-\alpha} + K(r\check{d})^{-\alpha})$. The probability of coverage

is thus given by

$$\eta_U^1 = 1 - \frac{(1-\tau)}{\Gamma(v)}\gamma\left(v, \frac{\tilde{\beta}\sigma_n^2}{p_c G_c w}\right) - \tau\frac{p_c G_c w}{\tilde{\beta}\bar{p}_r G_r}\left(\frac{1}{U^\alpha} + \frac{K}{\left(r\check{d}\right)^\alpha}\right)^{-1} \sum_{n=0}^{\infty}\left(1 + \frac{p_c G_c w}{\tilde{\beta}\bar{p}_r G_r}\left(\frac{1}{U^\alpha} + \frac{K}{\left(r\check{d}\right)^\alpha}\right)^{-1}\right)^{-(n+v+1)}. \quad (20)$$

In deriving the expression above, we assumed that there is no blockage on the path between the RIS at r and the UE at U as we substituted with the power gain of the combined (direct and indirect) channels between the UE and the base station, and between the UE and the radar. In reality, obstacles between the RIS and the UE may block the signal path and in this case, the problem reverts to the traditional system without the RIS (i.e., $\eta_U^1 \approx \eta_U^0$). The probability of path blockage P_{block} is an increasing function of the distance between the UE and the RIS, namely $\check{d} = |r - U|$ in the equations, such that

$$P_{block}(\check{d}) = 1 - \exp\left(-\psi\check{d}\right), \quad (21)$$

where $\psi \geq 0$ is a parameter that depends on the density of obstructions in the environment [42]. In the special case $\psi = 0$, the probability of blockage is always zero between the RIS and the UE. Taking the effect of P_{block} in the analysis, the average η_U^1 takes the following form

$$\bar{\eta}_U^1 = \left(1 - \exp\left(-\psi\check{d}\right)\right)\exp\left(\frac{-\tilde{\beta}d_0^\alpha\sigma_n^2}{p_c G_c}\right) \times \left((1-\tau) + \frac{\tau}{1 + \frac{\tilde{\beta}\bar{p}_r G_r}{p_c G_c}\left(\frac{d_0}{U}\right)^\alpha}\right) + \exp\left(-\psi\check{d}\right) \times \left(1 - \frac{(1-\tau)}{\Gamma(v)}\gamma\left(v, \frac{\tilde{\beta}\sigma_n^2}{p_c G_c w}\right) - \tau\frac{p_c G_c w}{\tilde{\beta}\bar{p}_r G_r}\left(\frac{1}{U^\alpha} + \frac{K}{\left(r\check{d}\right)^\alpha}\right)^{-1} \sum_{n=0}^{\infty}\left(1 + \frac{p_c G_c w}{\tilde{\beta}\bar{p}_r G_r}\left(\frac{1}{U^\alpha} + \frac{K}{\left(r\check{d}\right)^\alpha}\right)^{-1}\right)^{-(n+v+1)}\right). \quad (22)$$

IV. Radar Performance Analysis

In this section, we analyze the RIS effect on the radar performance, represented by the probabilities of target detection and false alarm. As explained in Subsection II-C, the signal $R^r(t)$ received at the radar receiver consists of the radar signal reflected from the target in addition to interference and noise. Following the Rayleigh channel model in Subsection II-B and assuming a fluctuating target [54], the magnitude of the received signal $|R^r|$ follows a Rayleigh distribution whose conditional PDF in the presence of a target is

$$f_{|R^r|}(l|\text{target}) = \frac{2l}{\sigma_s^2 + \sigma_i^2 + \sigma_n^2}\exp\left(-\frac{l^2}{\sigma_s^2 + \sigma_i^2 + \sigma_n^2}\right), \quad (23)$$

where σ_s^2, σ_i^2, σ_n^2 are the powers of the radar signal reflected from the target, the interference, and the noise, respectively. Similarly, the conditional PDF of the received signal in the absence of a target

$$f_{|R^r|}(l|\text{no target}) = \frac{2l}{\sigma_i^2 + \sigma_n^2}\exp\left(-\frac{l^2}{\sigma_i^2 + \sigma_n^2}\right). \quad (24)$$

Given a detection threshold T, the probability of target detection, denoted by P_{det}, is

$$P_{\text{det}} = \int_T^\infty f_{|R^r|}(l|\text{target})dl = \exp\left(-\frac{T^2}{\sigma_s^2 + \sigma_i^2 + \sigma_n^2}\right), \quad (25)$$

and the probability of false alarm, denoted by P_{FA}, is

$$P_{\text{FA}} = \int_T^\infty f_{|R^r|}(l|\text{no target})dl = \exp\left(-\frac{T^2}{\sigma_i^2 + \sigma_n^2}\right). \quad (26)$$

We assume that the radar keeps P_{FA} fixed at some required $\tilde{P}_{\text{FA}}$ by adjusting the detection threshold T according to the interference level as follows [54]

$$T = \sqrt{-(\sigma_n^2 + \sigma_i^2)\log\left(\tilde{P}_{\text{FA}}\right)}. \quad (27)$$

This adjustment is important because high false alarm rates overload the radar and drain its resources. Substituting with T from (27) in (25) gives the relation between P_{FA}, P_{det}, and φ, the SINR at the radar receiver, as follows

$$\varphi = \frac{\sigma_s^2}{\sigma_i^2 + \sigma_n^2} = \frac{\log\left(P_{\text{FA}}\right)}{\log\left(P_{\text{det}}\right)} - 1. \quad (28)$$

In the above expressions, $\sigma_n^2 = (4\pi/\lambda)^2\tilde{\sigma}_n^2$ and $\sigma_s^2 = \frac{n_p p_r G_r^2 \Omega}{4\pi d^4}$ is the power of the reflected radar signal from the target (i.e., the first term of $R^r(t)$ in (6)) where n_p is the number of coherently processed pulses. As for σ_i^2, its value changes depending on whether there is an RIS or not. In the following two subsections, we derive the probability of target detection in the two cases with and without an RIS in the system.

A. Probability of Target Detection Without an RIS

In the case without an RIS, the interference power, σ_i^2, comes solely from the direct (first) component of the base station interference in $R^r(t)$ in (6) as follows

$$\sigma_{i,0}^2 = p_c G_c G_r z^{-\alpha}. \quad (29)$$

Consequently, the probability of target detection given a fixed target false alarm probability $\tilde{P}_{\text{FA}}$ is obtained by substituting with (29) in (28) as follows

$$\log P_{\text{det}}^0 = \frac{1}{1 + \frac{\sigma_s^2}{\sigma_n^2 + \sigma_{i,0}^2}}\log\tilde{P}_{\text{FA}} = \frac{1}{1 + \frac{n_p p_r G_r^2 \Omega}{4\pi d^2(\sigma_n^2 + p_c G_c G_r z^{-\alpha})}}\log\tilde{P}_{\text{FA}}. \quad (30)$$

Generally, the radar operator sets a protection distance z in order to achieve an acceptable $\tilde{P}_{\text{det}}$. From (28), (29), and (30), the guard distance without an RIS, denoted by z_0 is lower bounded by

$$z_0 \geq \left(\frac{p_c G_c G_r}{\frac{n_p p_r G_r^2 \Omega}{4\pi\tilde{\varphi}d^4} - \sigma_n^2}\right)^{\frac{1}{\alpha}}, \quad (31)$$

where $\tilde{\varphi}$ is an SINR threshold calculated from (28) to achieve the required $\tilde{P}_{\text{det}}$ and $\tilde{P}_{\text{FA}}$.

B. Probability of Target Detection With an RIS

From the received radar signal in (6) in the presence of an RIS, the interference power denoted by $\sigma_{i,1}^2$ is

$$\sigma_{i,1}^2 = \sigma_{i,0}^2 + \Delta I_{rr} + \Delta I_{cr}, \tag{32}$$

where ΔI_{rr} is the additional interference from the scattering of the radar transmit signal back to the radar through the RIS, and ΔI_{cr} is the additional cellular interference from the base station through the RIS. The two terms are given as follows

$$\Delta I_{rr} = \frac{\bar{p}_r G_r^2}{4\pi} K r^{-2\alpha}, \tag{33}$$

$$\Delta I_{cr} = p_c G_c G_r K \left(r\hat{d}\right)^{-\alpha}. \tag{34}$$

Substituting with the interference from (32) in (28) gives the probability of target detection in the presence of RIS-assisted communication, which is

$$\begin{aligned}\log P_{\text{det}}^1 &= \frac{1}{1+\frac{\sigma_s^2}{\sigma_n^2+\sigma_{i,0}^2+\Delta I_{rr}+\Delta I_{cr}}} \log \tilde{P}_{\text{FA}} \\ &= \frac{\log \tilde{P}_{\text{FA}}}{1+\frac{n_p p_r G_r^2 \Omega}{4\pi d^2 \left(\sigma_n^2+p_c G_c G_r z^{-\alpha}+\frac{\bar{p}_r G_r^2}{4\pi} K r^{-2\alpha}+p_c G_c G_r K \left(r\hat{d}\right)^{-\alpha}\right)}}.\end{aligned} \tag{35}$$

It is seen from (32) that, for the same z, the radar always experiences higher interference, and hence lower probability of target detection, when an RIS is used. Accordingly, in order to make up for the extra interference caused by the RIS, the guard distance between the radar and the base station should increase if the base station is to use RIS-assisted communication. In addition, the RIS location between the base station and the radar affects not only the communication coverage of the base station, but also the radar performance as it affects the observed interference at the radar receiver. Consequently, the locations of the base station and the RIS should be optimized to maximize the performance of RIS-assisted communication without degrading the radar performance as presented in the next section.

V. Optimization of Base Station and RIS Placement

In this section, we optimize the placement of the base station and the RIS to maximize the probability of coverage of RIS-assisted communication while keeping the target detection probability at the radar unchanged compared to the traditional system without an RIS. The optimization problem is formulated as follows

$$\underset{a,z}{\text{maximize}} \quad : \quad \int_u \bar{\eta}_u^1 f_U(u) du \tag{36}$$

$$\text{subject to} \quad : \quad P_{\text{det}}^1 = P_{\text{det}}^0 \tag{37}$$

$$r = az \tag{38}$$

$$0 < a < 1 \tag{39}$$

The objective in (36) is the probability of coverage averaged over the UE positions over z and $f_U(u)$ is the PDF of the UE distribution. Constraint (37) guarantees that the radar probability of detection is unaffected by installing the RIS while constraints (38) and (39) indicate that the RIS should be installed between the base station and the RIS.

In order to keep P_{det}^1 in (35) the same as P_{det}^0 in (30), the optimum value of z (denoted by z^*) should be chosen such that

$$\sigma_{i,1}^2|_{z=z^*} = \sigma_{i,0}^2|_{z=z_0}. \tag{40}$$

Substituting with (29) and (32) in (40) gives the following polynomial of $(z^*)^{-\alpha}$:

$$q\,(z^*)^{-2\alpha} + (z^*)^{-\alpha} - z_0^{-\alpha} = 0 \tag{41}$$

where q is

$$q = \frac{K}{a^\alpha}\left(\frac{1}{(1-a)^\alpha} + \frac{\bar{p}_r G_r}{4\pi p_c G_c a^\alpha}\right), \tag{42}$$

and the required $(z^*)^{-\alpha}$ is the positive root of (41) as follows

$$z^* = \left(\frac{2q}{-1+\sqrt{1+\frac{4q}{z_0^\alpha}}}\right)^{\frac{1}{\alpha}}. \tag{43}$$

As seen from (42) and (43), z^* is a function of a. Consequently, substituting with $z = z^*$ and $r = az^*$ in (36) leaves only a to optimize such that the objective (36) is maximized subject to the constraint (39). Although the objective in (36) does not have a closed form, the optimization domain is small as $0 < a < 1$ and consequently, search-based solutions can be adopted. Algorithm 1 presents a simple selective search inspired by the heuristic evolutionary algorithms.

Algorithm 1 Selective Search Procedure

1: Initialize $\mathcal{A}$ to have N members in the range $(0,1)$.
2: **for** $a \in \mathcal{A}$ **do**
3: Calculate the fitness of a.
4: **end for**
5: **for** $i = 1 : N_{itr}$ **do**
6: Sort $\mathcal{A}$ in an ascending order according to the element value.
7: Set $\mathcal{B} = \emptyset$.
8: **for** $j = 1 : 2 : N$ **do**
9: Generate $x \sim U(0,1)$.
10: Generate child $b = x\mathcal{A}(j) + (1-x)\mathcal{A}(j+1)$.
11: Update $\mathcal{B} = \mathcal{B} + b$.
12: Calculate the fitness of b.
13: **end for**
14: Sort the members of $\mathcal{A} \cup \mathcal{B}$ in descending order according to their fitness.
15: Update $\mathcal{A}$ to be the N fittest members from Step 14.
16: **end for**
17: Choose $a^* = \mathcal{A}(1)$.

In Step 1, the algorithm initializes the parent population to include N samples from the interval $(0,1)$. Step 2 calculates the fitness of population $\mathcal{A}$. The fitness is taken to be the objective in (36). Steps 6-13 use $\mathcal{A}$ as a parent population to generate a child population $\mathcal{B}$ with $N/2$ members. First, the members of $\mathcal{A}$ are sorted in an ascending order according to their values. Then, in Steps 9-10, each two successive points

TABLE I
SIMULATION PARAMETERS

Radar	
Radar wavelength, λ	0.0833 m
Radar transmission power, p_r	850 kW
Radar antenna power gain, G_r	32 dBi
Reduction in antenna gain at the RIS/UE level	-2 dB
Radar range, d	50 km
Radar cross section of target, Ω	100
Pulse repetition frequency, ν	1.1 kHz
Pulse width, T_P	0.9 μs
Number of coherently processed pulses, n_p	100
Required probability of false alarm, $\tilde{P}_{\text{FA}}$	1×10^{-4}
Required probability of target detection, $\tilde{P}_{\text{det}}$	0.8
Communication	
Base station downlink transmit power, p_c	43 dBm
Base station antenna power gain, G_c	14 dBi
Number of RIS elements, K	1000
Noise power, σ_n^2	9×10^{-10}
Cellular SINR threshold, $\tilde{\beta}$	5 dB
Pathloss exponent, α	4
Frequency of UE exposure to radar interference, τ	0.25

are merged to generate a point that is randomly located in between (i.e., a child b with random traits from its parents). The newly generated point is added to the child population $\mathcal{B}$ (Step 11) and its fitness is calculated (Step 12). After that, in Step 14, the members of $\mathcal{A} \cup \mathcal{B}$ are sorted in a descending order according to their fitness and the new parent population $\mathcal{A}$ is updated in Step 15 to consist of the N fittest members (i.e., the survivors) from Step 14. The algorithm ends after N_{itr} iterations, and the optimum a (denoted by a^*), in Step 17, is chosen to be the fittest member of the surviving population.

VI. Numerical and Simulation Results

This section compares the analytical results with the results obtained from Monte-Carlo simulations using the simulation parameters in Table I. All simulations were conducted using MATLAB.

In the following two subsections, we show the effect of RIS deployment on the radar and communication performance compared to a traditional system without an RIS.

A. Radar Performance

Figure 2 shows how the RIS position between the radar and the base station affects the radar performance, represented by the interference at the radar receiver in Fig. 2(a) and the probability of target detection in Fig. 2(b). As observed from the figure, the deterioration in the radar performance is caused mainly by the ΔI_{rr} term in (32), which is the interference from the radar transmit signal scattered back to the radar through the RIS, and consequently the interference is particularly high (and the probability of detection is low) when the RIS is close to the radar. Furthermore, the interference increases slightly when the RIS gets close to the base station as it increases the interference through the indirect channel between the radar and the base station.

Figure 3 shows the optimum base station location z^* calculated using (43) for each relative position of the RIS a (i.e., $r = az^*$). The newly calculated z^* guarantees that deploying

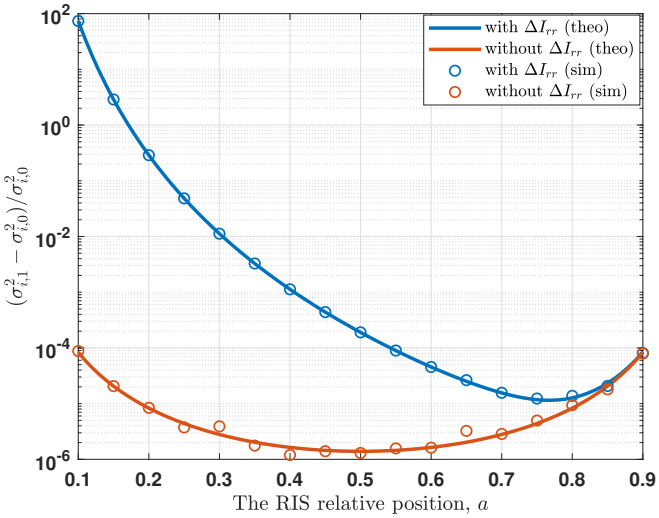

(a) Relative increase in the interference at the radar receiver.

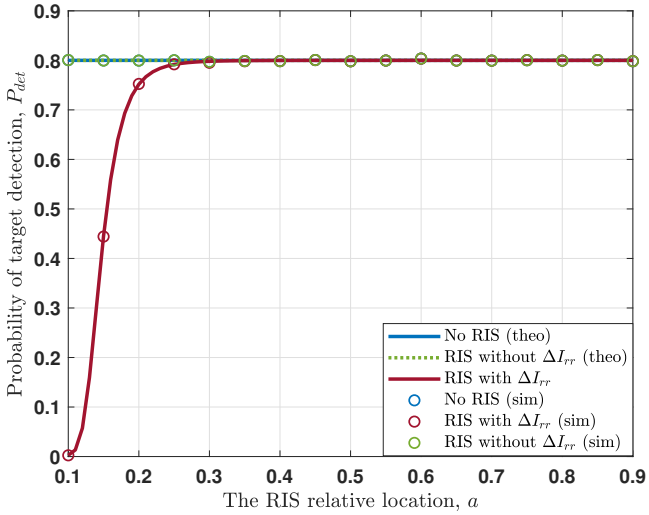

(b) Reduction in the probability of target detection.

Fig. 2. Effect of RIS relative position on the relative increase in the interference observed at the radar receiver.

an RIS does not increase the interference at the radar receiver compared to the traditional case without an RIS. As expected, if the RIS is located closer to the radar than to the base station (i.e., a is closer to 0), then z^* should be large in order to keep the RIS far enough from the radar. On the other hand, if the RIS is located closer to the base station than the radar (i.e., a is closer to 1), the term ΔI_{rr} can be neglected and consequently the protection distance does not need to increase (i.e., $z^* \approx z_0$)

Finally, Fig. 4 shows the interference at the radar receiver without an RIS, $\sigma_{i,0}^2$ and the interference $\sigma_{i,0}^2$ when an RIS is located at $r = az$. For each value of a, the value of z (base station location) is adjusted according to (43). As seen from the figure, using an RIS to assist the base station does not affect the interference level at the radar receiver, and hence its performance, as long as the base station location is optimized

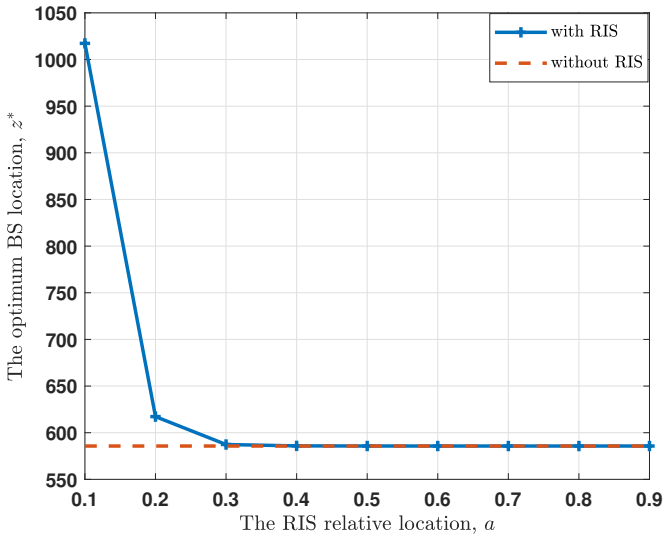

Fig. 3. The required base station location versus the relative location of the RIS.

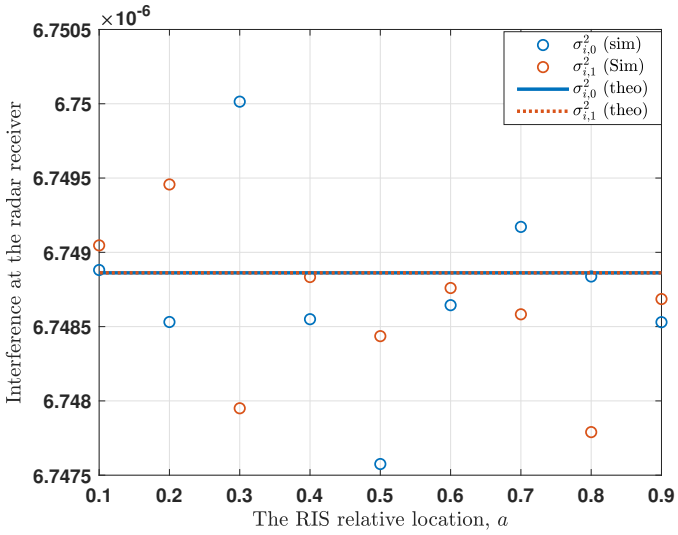

Fig. 4. Optimizing the base station location keeps the radar performance unaffected even when an RIS is used.

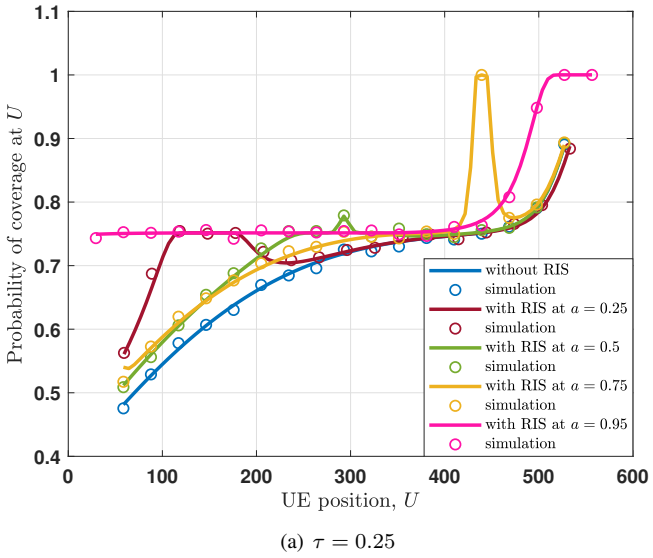

(a) $\tau = 0.25$

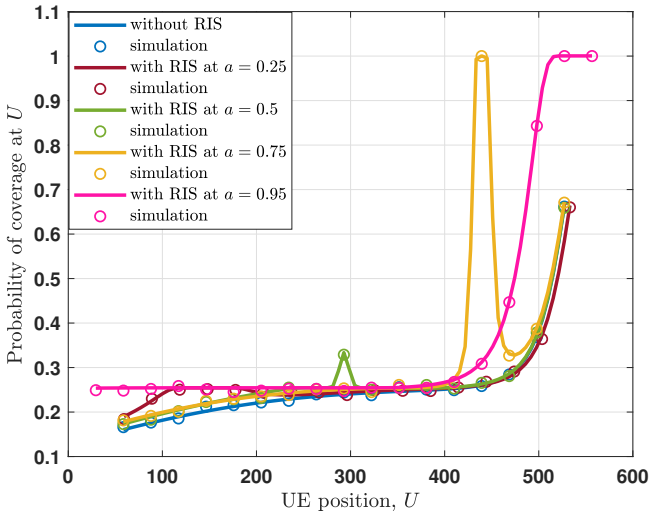

(b) $\tau = 0.75$

Fig. 5. Effect of RIS-assisted communication on the probability of coverage versus the UE position (at $\psi = 0$).

using (43).

B. Communication Performance

Fig. 5 shows the effect of RIS-assisted communication on the probability of coverage at different UE positions. It compares the case of non RIS-assisted communication (η_U^0 in (9)) with the case of an RIS deployed at $r = az$ (η_U^1 in (20)). We consider four different locations $a = 0.25, 0.5, 0.75$, and 0.95. In each case, z is calculated using (43) to keep the radar performance unaffected. Fig. 5(a) shows the case when the user experiences radar interference for 25% of the time (i.e., $\tau = 0.25$), and Fig. 5(b) shows the case when $\tau = 0.75$. As observed, generally, the probability of coverage improves as the UE moves closer to the base station and away from the radar due to increased signal strength and reduced interference. Also, the probability of coverage drops when τ increases as the radar interferes with the communication at the UE over a longer interval. Generally, communication is improved in the local region around the RIS due to signal improvement through beamforming. However, locating the RIS very close to the base station (e.g., $a = 0.95$) improves the coverage over the whole region because it minimizes the indirect pathloss from the base station to the UE at any location (i.e., $(\hat{d}\check{d})^{-\alpha} \approx d_0^{-\alpha}$). Moreover, it also maximizes the indirect path loss from the radar to any UE as the RIS is as far from the radar as possible. It is worth noticing that the results at $a = 0.95$ are quite optimistic as we assume that $\psi = 0$ (i.e., the path from the RIS to any UE is always unobstructed) and that there is no physical limitation to how close an RIS can be placed to the base station. Therefore the results at $a \approx 1$ serve as an upper bound to the potential performance of RIS-assisted communication.

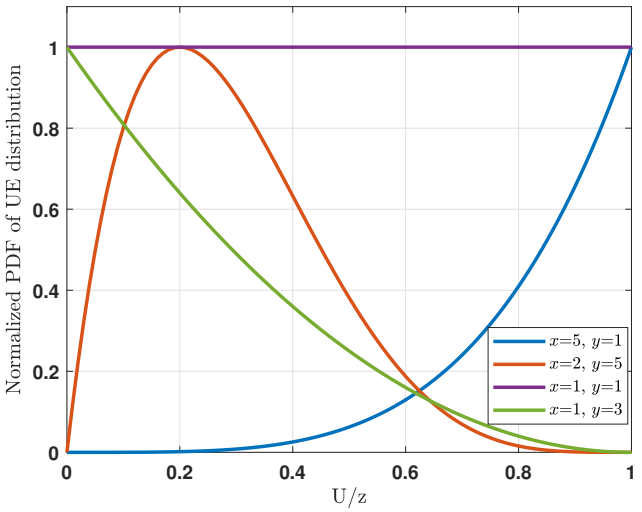

Fig. 6. UE distribution modeled using scaled Beta distribution with shape parameters x and y.

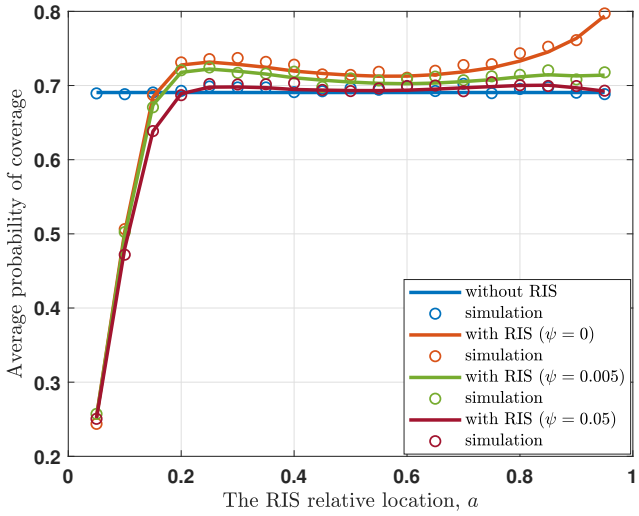

Fig. 7. Average probability of coverage versus the RIS relative location (at $x = 1$, $y = 1$).

We now focus our attention on the optimization problem in (36). We assume, without loss of generality, that UE positions follow a scaled Beta distribution whose PDF is

$$f_U(u) = \frac{\Gamma(x+y)}{\Gamma(x)\Gamma(y)} \frac{u^{x-1}}{z^x} \left(1 - \frac{u}{z}\right)^{y-1}, \quad 0 \le u \le z. \quad (44)$$

The distribution has a flexible shape that is controlled by the x and y parameters as shown in Fig. 6. From (44) and, as shown in Fig. 6, a UE is most likely to be in position $u = (x-1)/(x+y-2)$. The uniform distribution is a special case of (44) when $x = y = 1$.

Figs. 7- 10 show the effect of UE distribution on the optimum placement of the RIS. Different values of x and y are considered to represent different UE distributions over the exclusion zone. The figures sketch the average probability of coverage (i.e., the objective function (36)) versus the RIS relative location, a (i.e., the optimization variable). For each a, the base station location z is recalculated from (43) to keep the radar performance unaffected (i.e., to keep the constraint (37) satisfied). We also consider different values of P_{block} at $\psi = 0, 0.005$, and 0.05. The average probability of coverage of non-RIS assisted system appears as a horizontal line in the figures and is used as a baseline for comparison.

As seen in the figures, using a small a reduces the probability of coverage for two reasons: 1) the increased radar interference over the scattering channel between the RIS and the UEs and 2) the reduction in base station signal strength due to larger z (as shown in Fig. 3 and calculated from (43) to satisfy constraint (37)). As expected from Fig. 5, when $\psi = 0$, the RIS should be placed near the base station. The RIS improves the average probability of coverage by approximately 15%, 31%, 6%, 24%, respectively, in Figs. 7 - 10. We see that the highest improvements take place in the scenarios where most UEs are located close to the radar with bad base station coverage.

Obviously, increasing ψ limits the service or visibility range of the RIS, and consequently at $\psi = 0.005$, the optimum

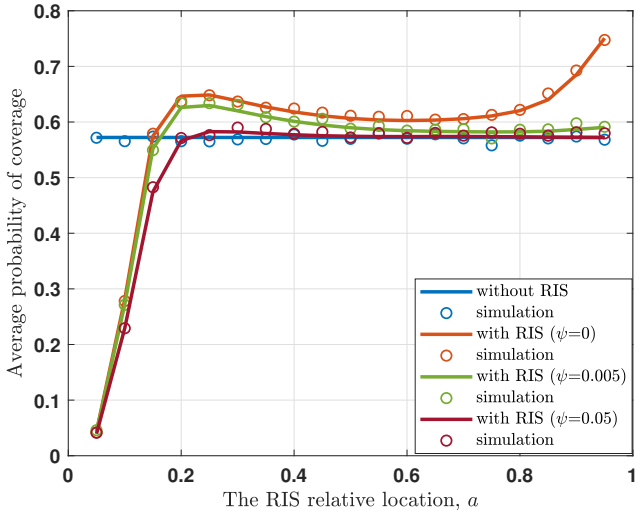

Fig. 8. Average probability of coverage versus the RIS relative location (at $x = 1$, $y = 3$).

placement of the RIS depends on the peak position of the UE distribution. For example, in Fig. 8, when $x = 1$ and $y = 3$, UEs are concentrated nearer to the radar than to the base station and consequently the best RIS location is closer to the radar than to the base station. Contrary to Fig. 8, the UE distribution considered in Fig. 9 has most of the UEs located near the base station not the radar, and consequently, the RIS should be placed near the BS where most UEs are located. In Fig. 10, the optimum RIS location is around $0.2Z$ where most UEs are located. Due to the limited visibility of the RIS, the improvement in the average probability of coverage drops to approximately 4%, 10%, 5%, 12%, respectively, in Figs. 7 - 10.

By increasing ψ further more to 0.05, the visibility range of the RIS becomes too limited such that it no longer affects the probability of coverage in most cases, and the improvement

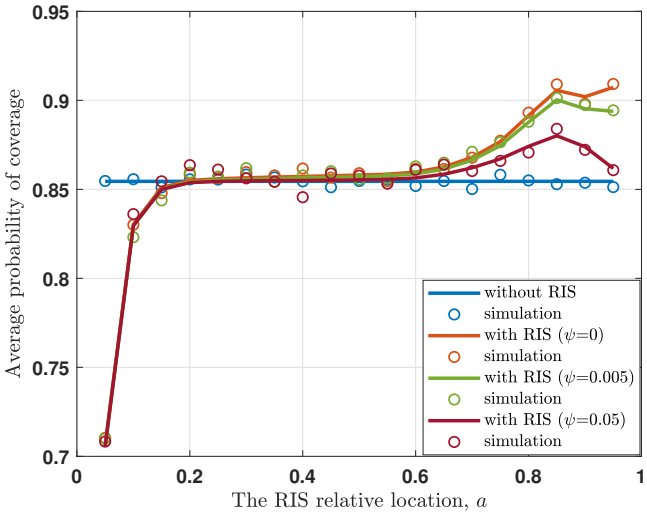

Fig. 9. Average probability of coverage versus the RIS relative location (at $x = 5$, $y = 1$).

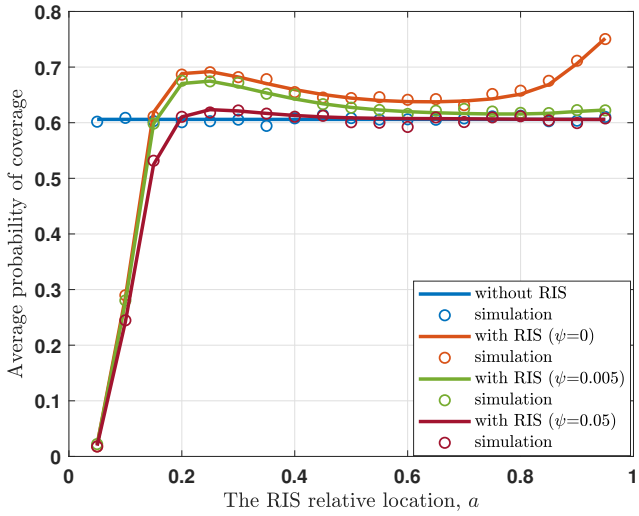

Fig. 10. Average probability of coverage versus the RIS relative location (at $x = 2$, $y = 5$).

in the average probability of coverage drops even more to approximately 1%, 2%, 3%, 3%, respectively, in Figs. 7 - 10. This case of frequent obstruction may require the installation of multiple RISs rather than a single RIS to guarantee that UEs in different locations can still connect to a nearby RIS.

VII. Conclusions and Future Work

This paper proposed using RISs to improve communication coverage near radars. Throughout the paper, we analyzed the effect of RIS deployment on the communication coverage and on the radar operation. We showed that optimizing the RIS and base station placement can enhance communication coverage without affecting the radar operation. The optimum locations depend on many factors including the UE distribution, the frequency of UE exposure to radar interference, and the required radar performance. A single RIS can improve communication coverage by 6-31% depending on the UE distribution, however the improvement diminishes by frequent obstruction of the path between the RIS and the UEs. In this case, it could be beneficial to use a number of RISs rather than a single RIS. A 2D stochastic geometry based framework to optimize the density of deployed RISs shall be considered in future work.

References

[1] "Harvesting unlicensed and shared spectrum: Opportunities and challenges," tech. rep., CTE•ISBE by Fontech, USA, GA., 2020.

[2] S. Parkvall, E. Dahlman, A. Furuskar, and M. Frenne, "NR: The new 5G radio access technology," *IEEE Communications Standards Magazine*, vol. 1, no. 4, pp. 24–30, 2017.

[3] D. Cohen, K. V. Mishra, and Y. C. Eldar, "Spectrum sharing radar: Coexistence via xampling," *IEEE Transactions on Aerospace and Electronic Systems*, vol. 54, no. 3, pp. 1279–1296, 2017.

[4] M. Chakraborty, B. Maji, and D. Kandar, "Dynamic spectrum access based simultaneous non-contiguous OFDM radar sensing and communication," *Microsystem Technologies*, vol. 27, no. 2, pp. 379–385, 2021.

[5] M. Kafafy, A. S. Ibrahim, and M. H. Ismail, "Stochastic geometry-based performance analysis of cellular systems in the vicinity of rotating radars," *IEEE Communications Letters*, vol. 25, no. 4, pp. 1391–1395, 2020.

[6] L. Zheng, M. Lops, and X. Wang, "Adaptive interference removal for uncoordinated radar/communication coexistence," *IEEE Journal of Selected Topics in Signal Processing*, vol. 12, no. 1, pp. 45–60, 2017.

[7] C. Wang, J. Tong, G. Cui, X. Zhao, and W. Wang, "Robust interference cancellation for vehicular communication and radar coexistence," *IEEE Communications Letters*, vol. 24, no. 10, pp. 2367–2370, 2020.

[8] C. Aydogdu, M. F. Keskin, N. Garcia, H. Wymeersch, and D. W. Bliss, "Radchat: Spectrum sharing for automotive radar interference mitigation," *IEEE Transactions on Intelligent Transportation Systems*, vol. 22, no. 1, pp. 416–429, 2019.

[9] M. F. Keskin, C. Aydogdu, and H. Wymeersch, "Stepped-carrier OFDM V2V resource allocation for sensing and communication convergence," in *EuCAP*, pp. 1–5, 2020.

[10] M. Kafafy, A. S. Ibrahim, and M. H. Ismail, "Maximum-service channel assignment in vehicular radar-communication," *IEEE Access*, vol. 9, pp. 138359–138370, 2021.

[11] A. Aubry, A. De Maio, Y. Huang, M. Piezzo, and A. Farina, "A new radar waveform design algorithm with improved feasibility for spectral coexistence," *IEEE Transactions on Aerospace and Electronic Systems*, vol. 51, no. 2, pp. 1029–1038, 2015.

[12] T. Tian, T. Zhang, G. Li, and T. Zhou, "Mutual information-based power allocation and co-design for multicarrier radar and communication systems in coexistence," *IEEE Access*, vol. 7, pp. 159300–159312, 2019.

[13] F. Wang, H. Li, and M. A. Govoni, "Power allocation and co-design of multicarrier communication and radar systems for spectral coexistence," *IEEE Transactions on Signal Processing*, vol. 67, no. 14, pp. 3818–3831, 2019.

[14] Y. Liu, Z. Wei, C. Yan, Z. Feng, and G. L. Stüber, "Effective capacity based power allocation for the coexistence of an integrated radar and communication system and a commercial communication system," *IEEE Access*, vol. 8, pp. 58629–58644, 2020.

[15] F. Liu, C. Masouros, A. Li, T. Ratnarajah, and J. Zhou, "MIMO radar and cellular coexistence: A power-efficient approach enabled by interference exploitation," *IEEE Transactions on Signal Processing*, vol. 66, no. 14, pp. 3681–3695, 2018.

[16] J. A. Mahal, A. Khawar, A. Abdelhadi, and T. C. Clancy, "Spectral coexistence of MIMO radar and MIMO cellular system," *IEEE Transactions on Aerospace and Electronic Systems*, vol. 53, no. 2, pp. 655–668, 2017.

[17] "Promoting investment in the 3550-3700 MHz band (da 18-538)," tech. rep., Federal Communications Comission, 2018.

[18] S. D. Blunt and E. S. Perrins, eds., *Radar and Communication Spectrum Sharing*. Radar, Sonar, and Amp Navigation, Institution of Engineering and Technology, 2018.

[19] F. Hessar and S. Roy, "Spectrum sharing between a surveillance radar and secondary Wi-Fi networks," *IEEE Transactions on Aerospace and Electronic Systems*, vol. 52, no. 3, pp. 1434–1448, 2016.

[20] M. Di Renzo, A. Zappone, M. Debbah, M.-S. Alouini, C. Yuen, J. De Rosny, and S. Tretyakov, "Smart radio environments empowered by reconfigurable intelligent surfaces: How it works, state of research, and the road ahead," *IEEE Journal on Selected Areas in Communications*, vol. 38, no. 11, pp. 2450–2525, 2020.

[21] E. Basar, M. Di Renzo, J. De Rosny, M. Debbah, M.-S. Alouini, and R. Zhang, "Wireless communications through reconfigurable intelligent surfaces," *IEEE access*, vol. 7, pp. 116753–116773, 2019.

[22] M. A. ElMossallamy, H. Zhang, L. Song, K. G. Seddik, Z. Han, and G. Y. Li, "Reconfigurable intelligent surfaces for wireless communications: Principles, challenges, and opportunities," *IEEE Transactions on Cognitive Communications and Networking*, vol. 6, no. 3, pp. 990–1002, 2020.

[23] S. Abeywickrama, R. Zhang, Q. Wu, and C. Yuen, "Intelligent reflecting surface: Practical phase shift model and beamforming optimization," *IEEE Transactions on Communications*, vol. 68, no. 9, pp. 5849–5863, 2020.

[24] C. Huang, A. Zappone, M. Debbah, and C. Yuen, "Achievable rate maximization by passive intelligent mirrors," in *ICASSP*, pp. 3714–3718, 2018.

[25] X. Yu, D. Xu, and R. Schober, "MISO wireless communication systems via intelligent reflecting surfaces," in *ICCC*, pp. 735–740, 2019.

[26] B. Ning, Z. Chen, W. Chen, and J. Fang, "Beamforming optimization for intelligent reflecting surface assisted MIMO: A sum-path-gain maximization approach," *IEEE Wireless Communications Letters*, vol. 9, no. 7, pp. 1105–1109, 2020.

[27] S. M. Razavizadeh and T. Svensson, "3D beamforming in reconfigurable intelligent surfaces-assisted wireless communication networks," in *WSA*, pp. 1–5, 2020.

[28] Z. Yang, M. Chen, W. Saad, W. Xu, M. Shikh-Bahaei, H. V. Poor, and S. Cui, "Energy-efficient wireless communications with distributed reconfigurable intelligent surfaces," *IEEE Transactions on Wireless Communications*, 2021.

[29] J. Ye, S. Guo, and M.-S. Alouini, "Joint reflecting and precoding designs for SER minimization in reconfigurable intelligent surfaces assisted MIMO systems," *IEEE Transactions on Wireless Communications*, vol. 19, no. 8, pp. 5561–5574, 2020.

[30] H. Han, J. Zhao, D. Niyato, M. Di Renzo, and Q.-V. Pham, "Intelligent reflecting surface aided network: Power control for physical-layer broadcasting," in *ICC*, pp. 1–7, 2020.

[31] J. Wang, W. Zhang, X. Bao, T. Song, and C. Pan, "Outage analysis for intelligent reflecting surface assisted vehicular communication networks," in *GLOBECOM*, pp. 1–6, 2020.

[32] D. Dampahalage, K. S. Manosha, N. Rajatheva, and M. Latva-aho, "Intelligent reflecting surface aided vehicular communications," in *GLOBECOM Workshops*, pp. 1–6, 2020.

[33] A. Al-Hilo, M. Samir, M. Elhattab, C. Assi, and S. Sharafeddine, "Reconfigurable intelligent surface enabled vehicular communication: Joint user scheduling and passive beamforming," *arXiv preprint arXiv:2101.12247*, 2021.

[34] Y. Chen, Y. Wang, J. Zhang, and Z. Li, "Resource allocation for intelligent reflecting surface aided vehicular communications," *IEEE Transactions on Vehicular Technology*, vol. 69, no. 10, pp. 12321–12326, 2020.

[35] S. Li, B. Duo, X. Yuan, Y.-C. Liang, and M. Di Renzo, "Reconfigurable intelligent surface assisted uav communication: Joint trajectory design and passive beamforming," *IEEE Wireless Communications Letters*, vol. 9, no. 5, pp. 716–720, 2020.

[36] L. Yang, F. Meng, J. Zhang, M. O. Hasna, and M. Di Renzo, "On the performance of RIS-assisted dual-hop uav communication systems," *IEEE Transactions on Vehicular Technology*, vol. 69, no. 9, pp. 10385–10390, 2020.

[37] S. Alfattani, W. Jaafar, Y. Hmamouche, H. Yanikomeroglu, A. Yongaçoglu, N. D. DJào, and P. Zhu, "Aerial platforms with reconfigurable smart surfaces for 5G and beyond," *IEEE Communications Magazine*, vol. 59, no. 1, pp. 96–102, 2021.

[38] K. Tekbıyık, G. K. Kurt, A. R. Ekti, A. Görçin, and H. Yanikomeroglu, "Reconfigurable intelligent surfaces empowered THz communication in LEO satellite networks," *arXiv preprint arXiv:2007.04281*, 2020.

[39] K. Tekbıyık, G. K. Kurt, A. R. Ekti, and H. Yanikomeroglu, "Reconfigurable intelligent surfaces in action for non-terrestrial networks," *arXiv preprint arXiv:2012.00968*, 2020.

[40] M. A. Kishk and M.-S. Alouini, "Exploiting randomly located blockages for large-scale deployment of intelligent surfaces," *IEEE Journal on Selected Areas in Communications*, vol. 39, no. 4, pp. 1043–1056, 2020.

[41] J. Lyu and R. Zhang, "Hybrid active/passive wireless network aided by intelligent reflecting surface: System modeling and performance analysis," *IEEE Transactions on Wireless Communications*, 2021.

[42] G. Ghatak, "On the placement of intelligent surfaces for RSSI-based ranging in Mm-Wave networks," *IEEE Communications Letters*, vol. 25, no. 6, pp. 2043–2047, 2021.

[43] K. Ntontin, A.-A. A. Boulogeorgos, D. Selimis, F. Lazarakis, A. Alexiou, and S. Chatzinotas, "Reconfigurable intelligent surface optimal placement in millimeter-wave networks," *arXiv preprint arXiv:2011.09949*, 2020.

[44] S. Zeng, H. Zhang, B. Di, Z. Han, and L. Song, "Reconfigurable intelligent surface (RIS) assisted wireless coverage extension: RIS orientation and location optimization," *IEEE Communications Letters*, vol. 25, no. 1, pp. 269–273, 2020.

[45] Y. U. Ozcan, O. Ozdemir, and G. K. Kurt, "Reconfigurable intelligent surfaces for the connectivity of autonomous vehicles," *IEEE Transactions on Vehicular Technology*, vol. 70, no. 3, pp. 2508–2513, 2021.

[46] H. Lu, Y. Zeng, S. Jin, and R. Zhang, "Enabling panoramic full-angle reflection via aerial intelligent reflecting surface," in *ICC Workshops*, pp. 1–6, 2020.

[47] Q. Zhang, W. Saad, and M. Bennis, "Reflections in the sky: Millimeter wave communication with uav-carried intelligent reflectors," in *GLOBECOM*, pp. 1–6, 2019.

[48] Z.-M. Jiang, M. Rihan, P. Zhang, L. Huang, Q. Deng, J. Zhang, and E. M. Mohamed, "Intelligent reflecting surface aided dual-function radar and communication system," *IEEE Systems Journal*, 2021.

[49] R. Sankar, B. Deepak, and S. P. Chepuri, "Joint communication and radar sensing with reconfigurable intelligent surfaces," *arXiv preprint arXiv:2105.01966*, 2021.

[50] X. Wang, Z. Fei, J. Guo, Z. Zheng, and B. Li, "RIS-assisted spectrum sharing between MIMO radar and MU-MISO communication systems," *IEEE Wireless Communications Letters*, vol. 10, no. 3, pp. 594–598, 2020.

[51] Y. Liu, X. Liu, X. Mu, T. Hou, J. Xu, M. Di Renzo, and N. Al-Dhahir, "Reconfigurable intelligent surfaces: Principles and opportunities," *IEEE Communications Surveys & Tutorials*, 2021.

[52] R. Saruthirathanaworakun, J. M. Peha, and L. M. Correia, "Opportunistic sharing between rotating radar and cellular," *IEEE Journal on Selected Areas in Communications*, vol. 30, no. 10, pp. 1900–1910, 2012.

[53] J. Salo, H. M. El-Sallabi, and P. Vainikainen, "The distribution of the product of independent rayleigh random variables," *IEEE transactions on Antennas and Propagation*, vol. 54, no. 2, pp. 639–643, 2006.

[54] M. Richards, J. Scheer, W. Holm, and W. Melvin, *Principles of modern radar: Basic principles*. SciTech Publishing, New Jersey, 2010.

Mai Kafafy received the PhD in 2019 from the Electronics and Communications Engineering Department in Cairo University. She is currently working as an Assistant Professor in the same department. Her research interests include wireless communication, machine learning, and signal processing.

Ahmed S. Ibrahim is currently an Assistant Professor at the Electrical and Computer Engineering Department at Florida International University (FIU), Miami, FL, USA. He received the B.S. and M.S. degrees in Electronics and Electrical Communications Engineering from Cairo University, Cairo, Egypt, in 2002 and 2004, respectively. He received the Ph.D. degree in Electrical Engineering from the University of Maryland, College Park, MD, USA, in 2009. He is a recipient of the NSF CAREER Award in 2022. Prior to joining FIU, Dr. Ibrahim was an assistant professor at Cairo University, wireless research scientist at Intel Corporation, and senior engineer at Interdigital Communications Inc. Dr. Ibrahim's research interests span various topics of wireless systems including drone-assisted millimeter wave communications, vehicular communications, and rethinking wireless networks through the lens of Riemannian geometry.

Mahmoud H. Ismail (S'00-M'07-SM'15) received the B.Sc. degree (with highest honors) in Electronics and Electrical Communications Engineering, the M.Sc. degree in Communications Engineering both from Cairo University, Egypt, in 2000 and 2002, respectively, and the Ph.D. degree in Electrical Engineering from The University of Mississippi, MS, USA, in 2006. From August 2000 to August 2002, he was a Research and Teaching Assistant in the Department of Electronics and Electrical Communications Engineering at Cairo University. From 2004 to 2006, he was a Research Assistant in the Center for Wireless Communications (CWC) at the University of Mississippi. He is currently a Full Professor at the American University of Sharjah, Sharjah, UAE and a Full Professor (on leave) at the Department of Electronics and Electrical Communications Engineering, Cairo University. He was also a Systems Engineering Consultant at Newport Media Inc. (now part of Microchip) in Cairo from 2006 - 2014. His research is in the general area of wireless communications with emphasis on performance evaluation of next-generation wireless systems and communications over fading channels. He is the recipient of the University of Mississippi Summer Assistantship Award in 2004 and 2005, The University of Mississippi Dissertation Fellowship Award in 2006, The University of Mississippi Graduate Achievement Award in Electrical Engineering in 2006 and the Best Paper Award presented at the 10th IEEE Symposium on Computers and Communications (ISCC 2005), La Manga del Mar Menor, Spain.